

Graphitic C₃N₄ Sensitized TiO₂ Nanotube Layers: A Visible Light Activated Efficient Antimicrobial Platform

Jingwen Xu,^a Yan Li,^a Xuemei Zhou,^b Yuzhen Li,^a Zhi-Da Gao,^a Yan-Yan Song^a and Patrik Schmuki^{bc}

a. College of Sciences, Northeastern University, Box 332, Shenyang 110004, China. E-mail: yysong@mail.neu.edu.cn. Tel.: +86-24-83687659.

b. Department of Materials Science, WW4-LKO, University of Erlangen-Nuremberg, Martensstrasse 7, D-91058 Erlangen, Germany. E-mail: schmuki@ww.uni-erlangen.de. Tel.: +49-9131-852-7575.

c. Department of Chemistry, Faculty of Science, King Abdulaziz University, P.O. Box 80203, Jeddah 21569, Saudi Arabia

This is the pre-peer reviewed version of the following article:

J. Xu, Y. Li, X. Zhou, Y. Li, Z.-D. Gao, Y.-Y. Song, P. Schmuki, Chem. Eur. J. 2016, 22, 3947

which has been published in final form at:

<http://onlinelibrary.wiley.com/doi/10.1002/chem.201505173/full>

DOI: 10.1002/chem.201505173

This article may be used for non-commercial purposes in accordance with Wiley Terms and Conditions for Self-Archiving.

Abstract:

In this work, we introduce a facile procedure to graft a thin graphitic C_3N_4 (g- C_3N_4) layer on aligned TiO_2 nanotube arrays (TiNT) by one-step chemical vapor deposition (CVD) approach. This provides a platform to enhance the visible-light response of TiO_2 nanotubes for antimicrobial applications. The formed g- C_3N_4 /TiNT binary nanocomposite exhibits excellent bactericidal efficiency against *E. coli* as a visible-light activated antibacterial coating.

Sterile or bactericidal surfaces are of a wide interest in healthcare related fields such as hospital environments.¹ There are several strategies to create a bacteria-free surface such as using disinfectant chemical treatments by alcohol, formaldehyde, or hydrogen peroxide,² or engineering antimicrobial coatings that contain bactericidal elements or compounds such as Ag, Cu, iodine, fluorine, phenol or heavy metals.³ However, many of these approaches provide only a time-limited antimicrobial activity,⁴ resistance to the anti-infectious agents,⁵ and can release toxic elements or compounds to environment.⁶

Another conceptually different strategy is to trigger bacterial inactivation by employing a photocatalytically active coating.⁷ Generally a number of photocatalysts can induce bacterial inactivation by the generation of highly reactive species (e.g. hydroxyl radicals and superoxides) or by direct valence band hole ejection that cause fatal damage to microorganisms.⁸ During the photocatalysis process, typically a decomposition of the cell membrane occurs, which can directly lead to the leakage of minerals, proteins, and genetic material, and thus results in cell death.⁹

As one of the most important photocatalysts, titanium dioxide (TiO_2) has attracted considerable attention in the antibacterial field, since its antimicrobial property was first reported in 1985.¹⁰ Titanium and its alloys are widely used in advanced medical applications such as orthopedics, dentistry, as well as components in medical devices and instruments. Thus the surface of such devices coated with a native or an anodic TiO_2 layer can show an intrinsic photocatalytic activity. Unfortunately, due to the wide band-gap of TiO_2 (~3.2 eV for anatase), the related photocatalytic properties (i.e. bacterial inactivation, self-cleaning and self-sterilization) need UV light to be triggered. TiO_2 is thus of a limited value, particularly in indoor environments (with low UV levels), such as in a hospital environment where preventing attachment and subsequent colonization of bacteria onto surfaces would be highly desired.¹¹ Therefore, strategies

to activate a visible-light photocatalytic response have become one of the most important issues in developing TiO₂ based antimicrobial coatings.¹²

Very recently, graphitic carbon nitride (g-C₃N₄), a polymeric semiconductor, has attracted considerable interest due to a band-gap of ~2.69 eV and its adequate band-positions for various red-ox reactions.¹³ However, its photocatalytic activity is unsatisfactory due to the low quantum efficiency.¹⁴ To resolve this problem, many attempts have been carried out to improve its photocatalytic performance, such as non-metal doping,¹⁵ preparation of nano/porous g-C₃N₄,¹⁶ and formation of band-gap matched heterojunction between g-C₃N₄ and other photocatalysts such as TiO₂, ZnO, and BiPO₄.¹⁷ Most of these studies have focused on the performance in the photocatalytic decomposition of organic pollutants and energy conversion.¹⁸ No work reported so far has dealt with the photocatalytic inactivation of bacteria under visible-light irradiation using g-C₃N₄ sensitized TiO₂ or other wide band-gap semiconductors or its use in an antimicrobial coating.

In the present work, we designed a one-step chemical vapor deposition (CVD) approach to deposit a small amount of g-C₃N₄ on aligned TiO₂ nanotube layers. Previous work showed that such nanotubular or nanoporous TiO₂ layers can be grown on a broad range of titanium geometries as well as on titanium alloys by a self-organizing electrochemical anodization process.¹⁹ These nanotubular or nanoporous structures provide highly defined nanoscale compartments that can be used as efficient payload scaffolds.²⁰ The g-C₃N₄ layer used here can be synthesized from a simple precursor via a polycondensation reaction (as outlined in the SI). We then studied the photocatalytic antibacterial property of the g-C₃N₄/TiNT nanocomposites under visible-light irradiation by inactivating of *Escherichia coli* (*E. coli*, a Gram-negative bacterium). The concept being illustrated in Fig. 1a relies on the photocatalytic generation of highly oxidative species that deactivate bacteria cells under visible light. The investigated approach offers a facile and cheap way to produce antibacterial surfaces and can be applied to a broad range of material surfaces. Thus it represents a promising coating for reducing infections (e.g. nosocomial infection in hospitals) and other indoor applications where only visible light is available.

Fig. 1b shows the SEM images of the TiNT layer grown on the Ti substrate. The aligned nanotube layers used in this work, with ~2.0 μm thickness and an average tube diameter of ~150 nm (Fig. 1b and 1c), are formed under optimized electrochemical anodization conditions (as

described in the Supporting Information, ESI*). In order to obtain an optimized photocatalytic activity, the amorphous TiO₂ nanotubes were converted to anatase by annealing in air. These tube layers were then decorated with g-C₃N₄ (as described in the SI). The SEM images in Fig. 1d and 1e clearly show that after the CVD decoration process the surface of the TiO₂ nanotubes is covered by patches of a g-C₃N₄ nanofilm. After deposition the colour of the samples changes from brown to black (see inset optical images in Fig. 1c and 1e).

These g-C₃N₄ loaded layers (in contrast to plain TiO₂ NT layers) show a visible light photo response as evident from photocurrent spectra. Fig. 1f shows photocurrent versus wavelength data recorded in a 0.1 M Na₂SO₄ aqueous solution (acquired as described in the SI) for nanotube layers loaded with different amounts of g-C₃N₄. The non-decorated tubes only show a UV response that corresponds to the band-gap of anatase of 3.2 eV. For the g-C₃N₄ loaded samples, in the visible-light region, the samples exhibit considerably enhanced photocurrents with an onset at ~2.4 eV. The highest visible response is obtained from a loading of 15 mg precursor. Therefore this loading was selected for further analysis and application. As shown in the X-ray diffraction (XRD) patterns of Fig. 1g, the appearance of a peak at 27.5° in g-C₃N₄/TiNT sample, which is corresponding to the interlayer stacking of aromatic segments, further confirms the formation of g-C₃N₄ on TiNT.

In Fig. 2a, the X-ray photoelectron spectroscopy (XPS) survey scan illustrates that the as-prepared sample contains elements of Ti, O, C and N. Fig. 2b shows the N 1s high-resolution spectrum, which is mainly composed of two peaks centered at 398.4 and 400.1 eV corresponding to the sp²-bonded N involved in the triazine rings (C-N=C) and the bridging N atoms in N-(C)₃, correspondingly.¹⁶ The small peak located at 403.7 eV is ascribed to the amino functions carrying hydrogen (N-H). Fig. 2c shows three peaks located at 284.8, 286.6, and 287.9 eV in the C 1s spectra. The peak at 284.6 eV is ascribed to sp² C=C bonds, the peak at 286.6 can be assigned to the sp² hybridized carbon atoms bonded to three nitrogen atoms in the g-C₃N₄ layer, and the peak at 287.9 eV is related to the sp² carbon atoms in the aromatic ring. The signals of O 1s (Fig. S1a, ESI*) and Ti 2p (Fig. S1b, ESI*) are typical of TiO₂ nanotubes. Additionally, FT-IR spectra of g-C₃N₄/TiNTs were also recorded in Fig. 2d. The broad bands in the 3000~3700 cm⁻¹ region are attributed to adsorbed H₂O molecules and N-H vibration modes from the uncondensed amine groups. The bands in the range of 1200~1600 cm⁻¹ relate to the stretching mode of C-N heterocycles. The sharp band observed at 804 cm⁻¹ is corresponding to the breathing mode of

triazine units. A typical band of TiO_2 can be seen at $\sim 470 \text{ cm}^{-1}$. These results confirm the successful synthesis and loading of $\text{g-C}_3\text{N}_4$ on TiO_2 nanotubes.

Concerning the prospective visible photocatalytic application of $\text{g-C}_3\text{N}_4/\text{TiNT}$ samples, the photo-induced inactivation of bacteria was investigated. *Escherichia coli* (*E. coli*), a typical bacterium responsible for many infections in daily life, is used as a model in the present work. The photocatalytic antibacterial activity of $\text{g-C}_3\text{N}_4/\text{TiNT}$ under visible light irradiation is evaluated in terms of the survival ratio of *E. coli*, which is defined as the ratio of the number of bacteria colonies present on the test surface and the number of colonies on a reference glass substrate (as glass substrates exhibit hardly any antibacterial activity). In Fig. 3a, the bare anatase and amorphous samples only show poor antibacterial activities with a survival ratio of $\sim 72\text{-}74\%$. Noticeably, the $\text{g-C}_3\text{N}_4/\text{TiNT}$ samples present a significantly improved antibacterial activity (the survival ratio of bacteria is only $\sim 16\%$) compared to the $\text{g-C}_3\text{N}_4$ decorated glass slide ($\text{g-C}_3\text{N}_4/\text{glass}$ shows a survival ratio of $\sim 86\%$ when irradiated by visible light). In addition, no obvious inactivation was observed in the dark control (catalysts without light irradiation) experiment, suggesting the nontoxicity of as-prepared $\text{g-C}_3\text{N}_4/\text{TiNT}$ nanocomposite to the *E. coli* cells during the test period. These results suggest that the photoinduced active species are the key for the bacterial inactivation on the $\text{g-C}_3\text{N}_4/\text{TiNT}$ antimicrobial coating, and the formation of $\text{g-C}_3\text{N}_4/\text{TiO}_2$ can promote the antibacterial efficiency in visible light.

To correlate the antibacterial efficiency with the photocatalytic activities of $\text{g-C}_3\text{N}_4/\text{TiNT}$ layers, the survival ratios were measured on a series of $\text{g-C}_3\text{N}_4/\text{TiNT}$ samples, which were prepared using different amounts of precursor. Fig. 3b shows the bacterial survival ratios as a dependence on the precursor loading (and for reference the visible light photocurrent response of these samples at 420 nm Fig. 3b). The results suggest that the bactericidal efficiency is directly related to the photocatalytic activity in visible light. The best bactericidal efficiency is achieved for the sample that reaches the highest visible photocurrent. In other words, these bactericidal results show that a loading of 15 mg of melamine is the optimal precursor amount for preparing highest efficiency $\text{g-C}_3\text{N}_4/\text{TiNT}$ layers.

The photocatalytic antibacterial activity of $\text{g-C}_3\text{N}_4/\text{TiNTs}$ was further studied for several bactericidal cycles (Fig. 3c). Some decrease of antibacterial activity in repeated cycles can be observed for the $\text{g-C}_3\text{N}_4/\text{TiNTs}$ samples – this may particularly originate from photocorrosion of

the g-C₃N₄ film under light irradiation for long periods as well as an accumulating coverage of the surface with dead bacterial cells (some dead bacterial cells remain attached to the coating surface even after washing the surface by ethanol and DI water thoroughly after each bactericidal cycle). In addition, the storage stability of g-C₃N₄/TiNTs samples is very high – the samples keep ~99% and 94% of their bactericidal activity against *E. coli* after being stored in dark and visible light ($\lambda > 450$ nm, $50 \mu\text{Wcm}^{-2}$) at room temperature for 3 months, respectively.

To illustrate the effect of g-C₃N₄/TiNT antibacterial coatings on the morphology of *E. coli*, we took SEM images before and after photo-inactivation (Fig 3d-e). Before illumination, *E. coli* cells present an intact cell structure and a well-defined rod shape. After the photocatalytic inactivation under visible-light irradiation (Fig. 3e), the outer membrane of bacteria cells exhibits severe damage.²¹ The optical images represent the density of survived *E. Coli* on the glass slide (Fig. 3d inset) and on g-C₃N₄/TiNT (Fig. 3e inset) after photocatalytic inactivation (the image are taken following incubation on solid LB medium for 24 h). Clearly, only a small percentage of bacteria colonies survive after the visible-light induced photocatalytic treatment on g-C₃N₄/TiNT. This result further illustrates the efficiency of inactivation of *E. coli* under visible-light irradiation using g-C₃N₄/TiNT coatings.

The assumed underlying mechanism for the anti-bacterial activity of the g-C₃N₄/TiO₂ system is outlined in Fig. 1a. It is based on a classic photocatalytic reaction scheme where the key is the creation of photo-promoted electrons that react with environmental O₂ to form superoxide radicals and related strong active oxidizers. In the present case g-C₃N₄ acts as visible light absorber (sensitizer, Fig. S2, ESI*) that (based on relative energetic positions of the band) forms a junction with TiO₂ that aids electron hole separation, and thus suppresses recombination. Electrons excited to either the g-C₃N₄ or the TiO₂ conduction band are energetically in a position that can react with environmental O₂ to form superoxide species (Fig. S3a, ESI*). In other words, the presence of oxygen in such a scheme is the key for reactivity. And indeed we find that the antibacterial activity of g-C₃N₄/TiNT decreases significantly (the bacterial survival ratio increased to ~ 60%) if the photocatalytic bacterial inactivation experiments are performed in anaerobic conditions (as an anaerobic bacteria, *E. coli* can live without oxygen).

Moreover, superoxide can react to OH• radicals. In order to detect the presence of OH•, we employed a classic fluorescence approach based on the reaction of OH• with terephthalic acid (TA) to form 2-hydroxyterephthalic acid (which shows a characteristic blue fluorescence at 426

nm) (Fig. S3b, ESI*).²² Under visible light illumination no obvious fluorescence can be detected for amorphous or anatase sample without g-C₃N₄ sensitizing. In contrast, for g-C₃N₄ hydroxyl radicals can be detected. Overall, these findings support the valence band mechanism outlined in **Fig. 1a**.

Conclusions

By combining TiO₂ nanotube layers and g-C₃N₄ nanofilms we have developed a binary nanocomposite which shows a significant bactericidal effect under visible light. The effect is based on the visible light induced photocatalytic formation of highly reactive oxidative species. These active species severely attack microorganisms, in our case *E. Coli*. However, we believe that the platform reported here can be used in a much wider range of visible light activated photocatalytic processes and applications.

Acknowledgements

This work was supported by the National Natural Science Foundation of China (No. 21322504, 21275026), the Fundamental Research Funds for the Central Universities (N140505001, N140504006), and the Program for Liaoning Excellent Talents in University (LJQ2013028). We also thank ERC, DFG and DFG-funcos for their support.

References

1. H. W. Boucher, and G. R. Corey, *Clin. Infect. Dis.*, 2008, **46**, S344.
2. J. W. Costerton, P. S. Stewart, and E. P. Greenberg, *Science*, 1999, **284**, 1318.
3. V. Sambhy, M. M. Macbride, B. R. Peterson, and A. Sen, *J. Am. Chem. Soc.*, 2006, **128**, 9798.
4. G. Donelli, and I. Fancolini, *J. Chemother.*, 2001, **13**, 595.
5. S. B. Lee, R. R. Koepsel, S. W. Morley, K. Matyjaszewski, Y. Sun, and A. J. Russell, *Biomacromolecules*, 2004, **5**, 877.
6. E. Kroke, and M. Schwarz, *Chem. Rev.*, 2004, **248**, 493.
7. O. Seddiki, C. Harnagea, L. Levesque, D. Mantovani, and F. Rosei, *Appl. Surf. Sci.*, 2014, **308**, 275.
8. M. R. Hoffmann, S. T. Martin, W. Choi, and D. W. Bahnemann, *Chem. Rev.*, 1995, **95**, 69.
9. Z. Lu, L. Zhou, Z. Zhang, W. Shi, Z. Xie, H. Xie, D. Pang, and P. Shen, *Langmuir*, 2003, **19**, 8765.

10. M. S. Hoffmann, T. Martin, W. Choi, and D. W. Bahnemann, *Chem. Rev.*, 1995, **95**, 69.
11. A. Fujishima, and K. Honda, *Nature*, 1972, **38**, 37.
12. (a) R. Asahi, T. Morikawa, T. Ohwaki, K. Aoki, and Y. Taga, *Science*, 2001, **293**, 269; (b) H. G. Kim, D. W. Hwang, and J. S. Lee, *J. Am. Chem. Soc.*, 2004, **126**, 8912.
13. E. Kroke, and M. Schwarz, *Chem. Rev.*, 2004, **248**, 493; F. Goettmann, A. Fischer, A. Thomas, and M. Antonietti, *Angew. Chem. Int. Ed.*, 2006, **45**, 4467.
14. Y. J. Zhang, T. Mori, J. H. Ye, and M. Antonietti, *J. Am. Chem. Soc.*, 2010, **132**, 6294.
15. J. Liang, Y. Zheng, J. Chen, J. Liu, D. Hulicova-Jurcakova, M. Jaroniec, and S. Z. Qiao, *Angew. Chem.*, 2012, **124**, 3958.
16. Y. J. Zhang, A. Thomas, M. Antonietti, X. C. Wang, and *J. Am. Chem. Soc.*, 2009, **131**, 50.
17. (a) L. Zhang, D. Jing, X. She, H. Liu, D. Yang, Y. Lu, J. Li, Z. Zheng, and L. Guo, *J. Mater. Chem. A*, 2014, **2**, 2071; (b) J. Wang, W. D. Zhang, and *Electrochimica Acta*. 2012, **71**, 10; (c) G. Z. Liao, S. Chen, X. Quan, H. T. Yu, and H. M. Zhao, *J. Mater. Chem.*, 2012, **22**, 2721.
18. W. J. Wang, C. J. Yu, D. H. Xia, P. K. Wong, and Y. C. Li, *Environ. Sci. Technol.*, 2013, **47**, 8724.
19. J. M. Macak, H. Tsuchiya, and P. Schmuki, *Angew. Chem. Int. Ed.*, 2005, **44**, 2100.
20. Y. Y. Song, F. Schmidt-Stein, S. Bauer, and P. Schmuki, *J. Am. Chem. Soc.*, 2009, **131**, 4230.
21. S.C. Roy, M. Paulose, and C.A. Grimes, *Biomaterials*, 2007, **28**, 4667.
22. (a) T. Hirakawa, and Y. Nosaka, *Langmuir*, 2002, **18**, 3247; (b) K. Ishibashi, A. Fujishima, T. Watanabe, K. Hashimoto, *J. Photochem. Photobiol. A: Chem.*, 2000, **134**, 139.

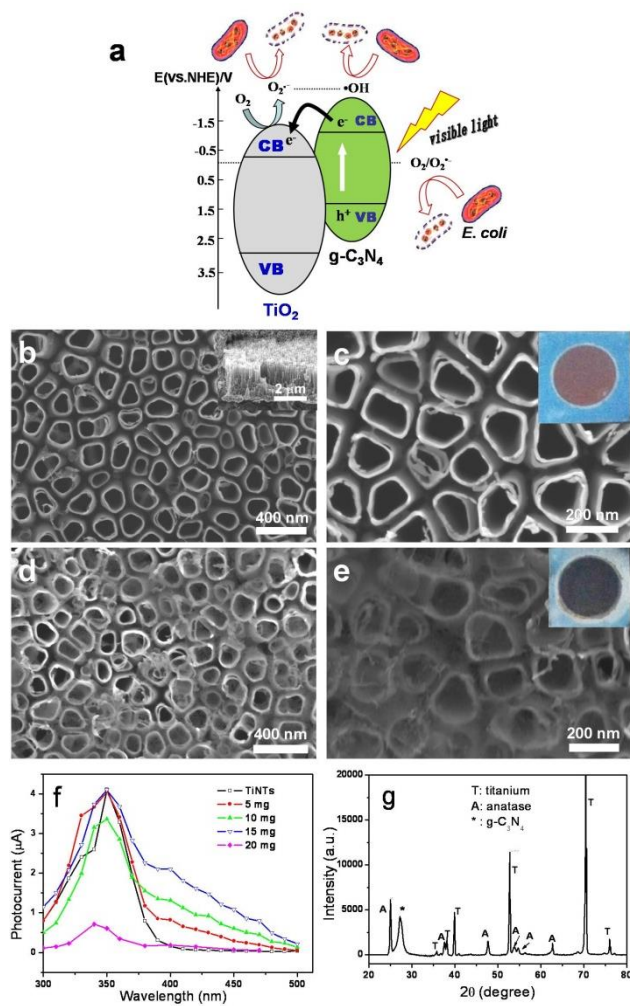


Fig. 1 (a) Scheme for the photocatalysis induced antibacterial mechanism of g-C₃N₄/TiNT under visible-light illumination. SEM images: top view of TiNT layer (b and c) and g-C₃N₄/TiNT layer (d and e). Insert: cross-sectional view of bare TiO₂ nanotube arrays and corresponding optical images for TiNT layer and g-C₃N₄/TiNT layer. (f) Photocurrent-wavelength responses of TiNTs and g-C₃N₄/TiNTs prepared from different amount of melamine as a precursor at a bias of +0.5 V (vs SCE) in 0.1 M Na₂SO₄. (g) XRD patterns of g-C₃N₄/TiNT layers prepared at 550 °C.

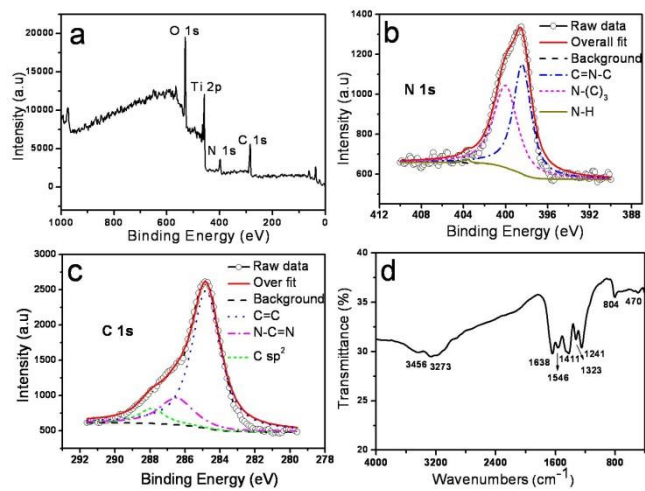


Fig. 2 (a) XPS survey spectrum of g-C₃N₄/TiNTs, (b) N 1s and (c) C 1s for g-C₃N₄/TiNT, and (d) FT-IR spectrum of g-C₃N₄/TiNT.

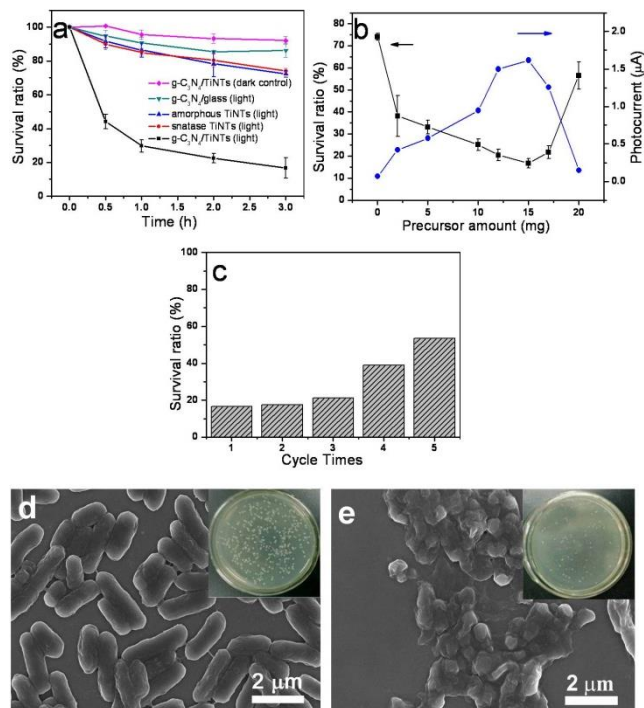


Fig. 3 (a) Survival ratio of *E. coli* on g-C₃N₄/glass, amorphous TiNT, anatase TiNT, and g-C₃N₄/TiNT layers by irradiating under visible-light, and the survival ratio of *E. coli* on g-C₃N₄/TiNT layers in dark. (b) The influence of dosage of melamine on the photocurrent (at 420 nm) of as-formed g-C₃N₄/TiNT samples and the survival ratio of *E. coli* after irradiated by visible light for 3 h. (c) The survival ratio *E. coli* on optimized g-C₃N₄/TiNTs sample under visible-light irradiation for five cycles. SEM images of *E. coli* without (d) and with (e) photoinduced inactivation on g-C₃N₄/TiNT surface by visible-light irradiation. The corresponding optical images of survival *E. coli* after incubation on solid LB medium at 37 °C for 24 h: (d inset) without and (e inset) with photoinduced inactive treatment on g-C₃N₄/TiNT surface by visible-light irradiation.

Electronic Supplementary Information

Graphitic C₃N₄ Sensitized TiO₂ Nanotube Layers: A Visible Light Activated Efficient Antimicrobial Platform

Jingwen Xu,^a Yan Li,^a Xuemei Zhou,^b Yuzhen Li,^a Zhi-Da Gao,^a Yan-Yan Song,^{a*} Patrik Schmuki^{b*}

^a College of Sciences, Northeastern University, Box 332, Shenyang 110004, China

^bDepartment of Materials Science, WW4-LKO, University of Erlangen-Nuremberg, Martensstrasse 7, D-91058, Erlangen, Germany

Experimental Section

Preparation of TiO₂ nanotube arrays

Ti foils (99.6% purity) were cleaned in ethanol and deionized water (DI) by sonication, and then dried with a nitrogen stream. The cleaned Ti foils were pressed together with a Cu plate against an O-ring sealed opening in an electrochemical cell (with 0.5 cm² exposed to the electrolyte) and then anodized in a glycerol/water (50:50) electrolyte with 0.27 M NH₄F at 30 V for 4 h at room temperature. Ti foils served as the working electrode, and a platinum sheet was used as the counter electrode. The as-formed TiNT layers were annealed in air at 550 °C for 1 h to crystallize the TiO₂ to anatase before further decoration.

Preparation of g-C₃N₄/TiNT samples

g-C₃N₄ decoration was performed by a chemical vapor deposition (CVD) approach using melamine as a precursor. Specifically, a defined amount of melamine was added into a combustion boat with the TiNT layer top-down placed above the melamine powders (distance ≈ 1.0 cm). The system was sealed and heated at 550 °C for 3 h to decorate the TiNT with the g-C₃N₄ polymer, and the as-prepared g-C₃N₄/TiNT samples were then stored in dark before experiment. The g-C₃N₄/glass samples were prepared in a similar way, but replacing the TiNT substrate with a glass slide (with a roughened surface by grinding) of the same surface area as the TiNT samples.

Antibacterial test

Gram-negative *Escherichia coli* (*E. coli*) DH5 α were selected as the model target microorganism for antibacterial tests. Before microbiological experiments, all glass ware was sterilized by autoclaving at 121 °C for 20 min. A 300 W xenon lamp with a UV cutoff filter ($\lambda < 420$ nm) was used as light source for photocatalysis induced antibacterial study. For antibacterial experiments, 100 μ L mixture of liquid Luria broth (LB) substrate containing 0.5% agar and 10⁵ colony-forming unites per milliliter (CFU mL⁻¹) of *E. coli* was dropped onto the surface of g-C₃N₄/TiNT or TiNT samples. The light source was located 20 cm from the samples (50 mW cm⁻² illumination intensity). To quantify the antimicrobial results, the semi-solid bacteria solution was withdrawn after the photoinactivation step and then diluted serially with sterilized Milli-Q water to adjust the bacterial concentration (the aliquots were diluted to 10⁻⁴ times in our present study) to ensure the growing bacterial colonies were legible. Then 100 μ L of the treated solution was spread on solid LB medium. The colonies were continued to incubate at constant temperature of 37 °C for 24 h, and then counted to determine the survival bacteria numbers and bactericidal efficiency. For better comparison, bactericidal efficiency of amorphous and anatase TiNT layers was also studied by the same procedure. The survival ratio was determined by comparing the survival colony counts with the corresponding colony counts

of control sample (sterilized glass sheet). All of the photocatalytic antibacterial experiments were repeated three times to give an average value.

Trapping experiments for radicals and holes

For the trapping of radicals and holes, 4 mL RhB (2 mg L^{-1}) solution was photodegraded by g-C₃N₄/TiNT layer under visible light (a 300 W xenon lamp with a UV cutoff filter $\square\square\square\square 420 \text{ nm}$). The trapping experiments were carried out by adding benzoquinone (1.0 mmol L^{-1} , superoxide radical scavenger), ethylene diamine tetraacetic acid (10 mmol L^{-1} , hole scavenger), and methanol (1/15 volume ratio, hydroxyl radical scavenger) separately to get rid of radicals and holes during the photocatalysis process under visible-light irradiation. UV spectra were used to detect the degradation of RhB with time [S1-S4].

The generated hydroxyl radicals were detected by fluorescence (FL) spectra by using terephthalic acid (TA) as a probe molecule. The g-C₃N₄/TiNT sample was immersed into a 4 mL aqueous solution with terephthalic acid (3 mM), NaCl (0.1 M) and NaOH (0.01 M), and the FL spectra of the solution were measured for every 10 min with excitation wavelength at 315 nm [S5-6].

Apparatus

The morphologies of the g-C₃N₄/TiNT samples and bacteria were characterized using a field-emission scanning electron microscope (Hitachi FE-SEM S4800). X-ray photoelectron spectra (XPS) were recorded on a Perkin–Elmer Physical Electronics 5600 spectrometer. All the peaks are shifted with a standard of C 1s at 284.8 eV. The UV-vis absorption spectra were measured on a spectrophotometer (Perkin–Elmer, Lambda XLS+, USA). The photocurrents were recorded by measuring at 420 nm in an aqueous solution containing 0.1 M Na₂SO₄ with an applied bias of +0.5 V (vs saturated calomel electrode (SCE)).

References:

- [S1] C. Richard, P. Boule, *Sol. Energy Mater. Sol. Cells.*, 1995, 38, 431;
- [S2] N. Shimizu, C. Ogino, M. F. Dadjour, T. Murata, *Ultrason. Sonochem.*, 2007, 14, 184;
- [S3] Y. Sun, J. J. Pignatello, *Environ. Sci. Technol.*, 1995, 29, 2065;
- [S4] N. Serpone, I. Texier, A.V. Emeline, P. Pichat, H. Hidaka, J. Zhao, *J. Photochem. Photobiol. A: Chem.*, 2000, 136, 145;
- [S5] K. Ishibashi, A. Fujishima, T. Watanabe, K. Hashimoto, *J. Photochem. Photobiol. A: Chem.*, 2000, 134, 139;
- [S6] T. Hirakawa, and Y. Nosaka, *Langmuir*, 2002, 18, 3247.

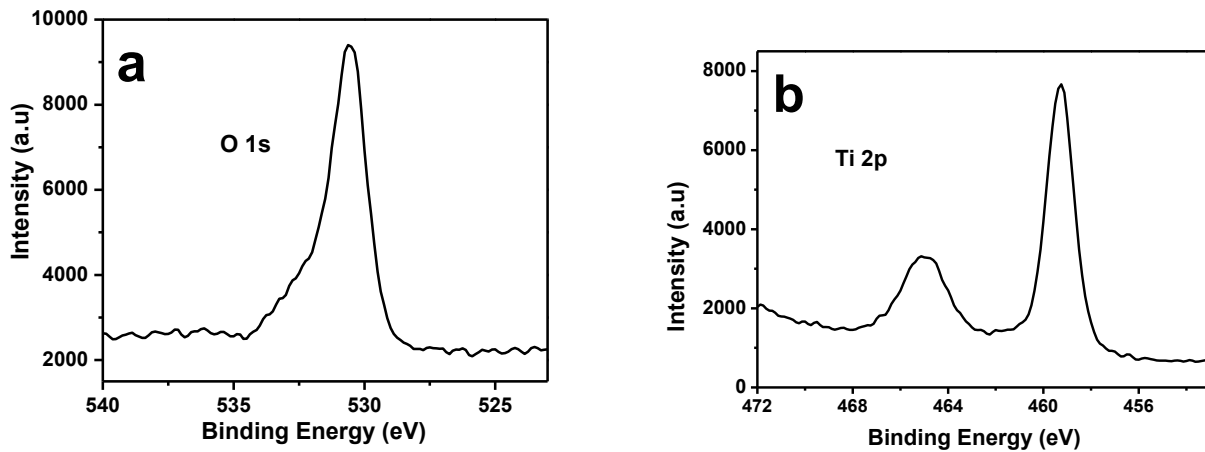


Fig. S1. XPS (a) O 1s and (b) Ti 2p spectra of g-C₃N₄/TiNTs layer.

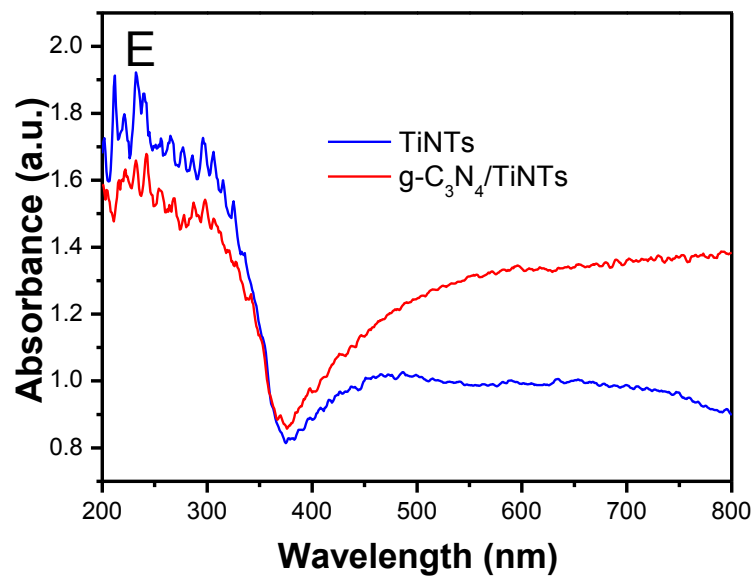


Fig. S2. UV-visible diffuse reflectance spectra of TiNT and g-C₃N₄/TiNT.

To evaluate visible-light activity introduced by the g-C₃N₄ decoration, we acquired reflectivity data. As shown in Fig. 2D, the decoration of g-C₃N₄ results in an obviously enhanced absorption in visible range.

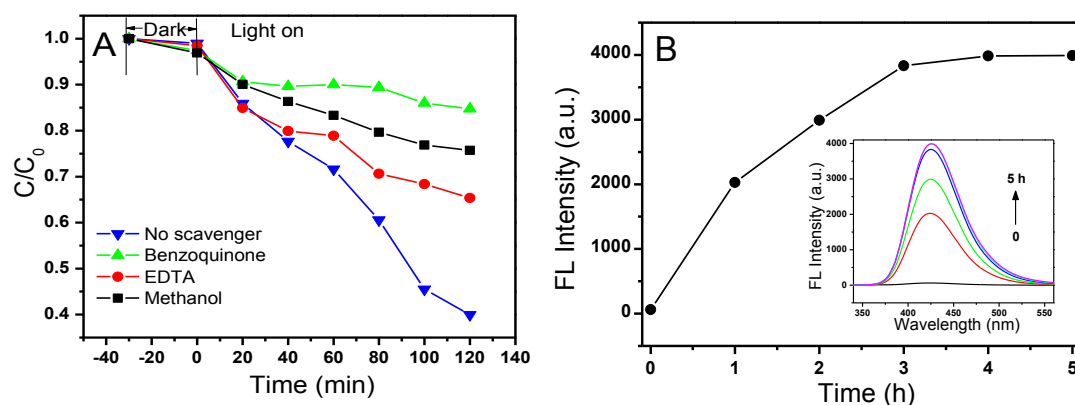


Fig. S3 (A) Influence of different scavengers on the photocatalytic degradation of RhB by $g\text{-C}_3\text{N}_4/\text{TiNT}$ samples under the irradiation of visible light. (B) Fluorescence intensity at 426 nm measured from the supernatant solution of terephthalic acid after irradiate $g\text{-C}_3\text{N}_4/\text{TiNT}$ by visible light for different time. Insert: The time dependence fluorescence spectra.

In Fig. S3a, the photodegradation of organic dye (2 mg L^{-1} RhB) is performed under visible light to further elucidate the possible reactive species that are directly involved in the damage of bacterial cells or organic molecules during the photocatalysis process. A significant decline in the photodegradation efficiency is observed when methanol (the scavenger agent for hydroxyl radicals), EDTA (the scavenger agent for holes) and benzoquinone (the scavenger agent for superoxide radicals) are separately added into the RhB solution. These results demonstrate that all the reactive species take part in the photocatalysis process, the superoxide radicals having the strongest influence [S1-S4]. Fig. S3b shows the increased fluorescence signals with irradiation time when $g\text{-C}_3\text{N}_4/\text{TiNT}$ layer is illuminated by visible light in a TA containing solution. This result demonstrates the formation of hydroxyl radicals during the photocatalytic process [S5-6].